



Preparation of MoSe₂ nano-islands array embedded in a TiO₂ matrix for photo-regulated resistive switching memory



Pengde Han ^{a,*}, Bai Sun ^b, Sen Cheng ^a, Fangli Yu ^a, Baoxiang Jiao ^a, Qisheng Wu ^a

^a School of Materials Engineering, Yancheng Institute of Technology, Yancheng 224051, China

^b School of Physics Science and Technology, Southwest University, Chongqing 400715, China

ARTICLE INFO

Article history:

Received 9 November 2015

Received in revised form

6 December 2015

Accepted 15 December 2015

Available online 31 December 2015

Keywords:

Resistive switching

Photo-controlled memory

MoSe₂ nano-islands

TiO₂ matrix

Anodic aluminum oxide (AAO) template

ABSTRACT

The electrically driven resistance change of a material, called memristive switching, is a fascinating phenomenon in the development of next generation nonvolatile memory alternatives to flash technology. Herein, the composite of MoSe₂ nano-islands array inserted into TiO₂ matrix grown on fluorine-doped tin oxide (FTO) substrate was prepared by anodic aluminum oxide (AAO) template assisted radio frequency magnetron sputtering. Further, a photo-controlled resistive switching memory device with Ag/[MoSe₂/TiO₂]/FTO structure is demonstrated. The device presents stable resistive switching memory behaviors in dark and under illumination respectively. Finally, the mechanism for the photo-controlled memory behaviors is discussed in detail. This implication provides a foundation for exploring the multifunctional composites and their applications in photo-controlled nonvolatile memory devices.

© 2015 Elsevier B.V. All rights reserved.

1. Introduction

Memristive switching phenomena at simple metal/oxide/metal junctions have attracted much attention due to not only fundamental interest in the mechanisms but also the potential uses in high-density universal memory devices, which has stimulated extensive research for exploring new functional materials and their applications in non-volatile memory devices [1–5]. Recently, resistive switching in many transition metal oxides has been observed and becomes the basis for the development of novel non-volatile resistive random access memory (RRAM) [6]. In the exploration of mechanism, the resistive switching effect is interface-related and takes place at the interface between metal electrode and the oxide materials. The interface plays a key role in the presence of oxygen vacancies that modulate the interface resistance [7–10]. However, the nanoscale physical and chemical origins of resistive switching are still under debate.

Recently, photo as new control method in the resistive switching has been reported [11–14]. The extra control parameter (photo-control) in the resistive switching can greatly broaden its applications. Indeed, the light-illumination conditions are particularly

attractive because optical signals are easier to apply over long distances than electrical signals, and optical signals can efficiently manage the interactions between circuit devices without disruption by signal interference.

During the last decade, as graphene and its related applications have stimulated many studies, numerous other two-dimensional materials have attracted great interest due to their unique properties and different energy band gaps compared to bulk material [15,16]. In recent investigations, new two-dimensional materials, such as MoSe₂, have been utilized in a variety of important applications [15–20]. It is truly worthy of note that MoSe₂ is an indirect semiconductor with a band gap of 1.7–1.9 eV [21–23]. The layers of Se–Mo–Se interact with each other through van der Waals forces. In addition, the typical synthesis routes, such as chemical vapor deposition, electro deposition, spray pyrolysis, physical vapor deposition and hydrothermal method, have been used widely for the preparation of MoSe₂ nanostructures [24–29].

Although the preparation of individual MoSe₂ and TiO₂ has been intensively investigated, the resistive switching memory properties of MoSe₂/TiO₂ composite have not been reported yet. In order to explore new developments and applications of the MoSe₂ material, in this work, MoSe₂ and TiO₂ powder were firstly synthesized by hydrothermal method, then the self-assembly MoSe₂ nano-islands array inserted into TiO₂ matrix grown on fluorine-doped tin oxide (FTO) substrate was prepared by anodic aluminum oxide (AAO)

* Corresponding author.

E-mail address: hanpengde@163.com (P. Han).

template assisted radio frequency magnetron sputtering, and the electrodes of Ag were made by vacuum deposition. The preparation process is shown in Fig. 1. In addition, Ag/[MoSe₂/TiO₂]/FTO structure device displays an excellent photo-controlled bipolar resistive switching behaviors, indicating the MoSe₂/TiO₂ composite holds promise for practical applications of photo-controlled RRAM devices.

2. Experimental procedure

2.1. Preparation of MoSe₂ and TiO₂ powder

In this work, MoSe₂ powder was synthesized by a hydrothermal method. Analytical sodium molybdate (Na₂MoO₄·2H₂O) and selenium (Se) of analytical grade were used as precursor reagents without any further purification. A stoichiometric amount of Na₂MoO₄·2H₂O and Se powder was put into a stainless steel autoclave with a 50 ml capacity with stirring until completely dissolved. Then an appropriate amount of hydrazine hydrate (N₂H₄·H₂O) was added into the tank under stirring. Distilled water was added to fill the autoclave up to 80% of the total volume under vigorous stirring for 30 min, and then the pH value was adjusted to about 12 with the addition of solid NaOH. The autoclave was sealed and maintained at 180 °C for 48 h, and then cooled to room temperature naturally. A black precipitate was collected. After being washed with absolute ethanol and distilled water, the final product was dried in a vacuum box at 60 °C for overnight. Finally, we made a target of magnetron sputtering using as-prepared MoSe₂ powders.

The TiO₂ powder was prepared using the sol–gel method. TiO₂ powder was synthesized using titanium(IV) isopropoxide (TIP) (Aldrich Chemical, Sigma–Aldrich Corporation, St. Louis, MO, USA), nitric acid, ethyl alcohol, and distilled water. The TIP was mixed with ethanol, and distilled water was added drop by drop under vigorous stirring for 1 h. This solution was then peptized using nitric acid and heated under reflux at 80 °C for 8 h. After this period, a TiO₂ sol was prepared. The prepared sol was dried to yield a TiO₂ powder. The TiO₂ particles were annealed in air at 450 °C for 1 h using a programmable furnace to obtain the desired TiO₂ stoichiometry and crystallinity. Similarly, we made a target of magnetron sputtering using as-prepared TiO₂ powders.

2.2. Preparation of Ag/[MoSe₂/TiO₂]/FTO structure device

Anodic aluminum oxide (AAO) membranes with ~200 nm pore size were fabricated by a two-step anodization of electropolished Al

sheets. The first anodization of Al sheet in 0.3 M H₂C₂O₄ solution was conducted for 12 h at 5 °C. The anodized Al sheet was completely removed in an aqueous acid mixture of H₃PO₄ and CrO₃ (6 wt% and 1.8 wt%) at 60 °C for 12 h. The second anodization was carried out for 3 min at 5 °C. The etching process in HgCl₂ at room temperature detached the alumina layer from the Al sheet. In sequence, the barrier layer was removed by the pore widening process with 5 wt% H₃PO₄ at 30 °C for 20 min. Finally, we obtained 500 nm-thick AAO membranes that provided excellent contacts with substrates.

MoSe₂ nano-islands were fabricated on FTO substrates through AAO nano-template by radio frequency magnetron sputtering method. The MoSe₂ nano-islands were deposited at room temperature and the power of the radio frequency was set at 80 W. The deposition rate of MoSe₂ was 0.02 nm s⁻¹. The typical base chamber pressure for the deposition was 5.0 × 10⁻⁵ Pa and the Ar working chamber pressure was 1.0 Pa. After MoSe₂ deposition, extended arrays of MoSe₂ nano-islands were obtained by mechanically lifting off the AAO mask. Then TiO₂ film with the thickness of ~200 nm was deposited on interspace of MoSe₂ nano-islands at room temperature. Finally, the electrodes with the area of ~1 mm² and the thickness of ~200 nm were deposited on the same side for the electric measurement by vacuum deposition.

2.3. Material characteristics

Microstructure of MoSe₂/TiO₂ compound was characterized by X-ray diffraction (XRD, Shimadzu XRD-7000 X-ray diffractometer) with Cu K α radiation. Surface morphology and energy dispersive X-ray spectroscopy (EDX) spectra of MoSe₂/TiO₂ compound grown on FTO substrate was characterized using scanning electron microscopy (SEM, JSM-6510). The microstructure characterization of the MoSe₂/TiO₂ compound was tested by transmission electron microscopy (JEM-2100) at an acceleration voltage of 200 kV. The chemical state was analyzed by X-ray photoelectron spectroscopy (XPS/ESCALAB250).

2.4. Device characteristics

In the test of resistive switching characteristics, Ag and FTO is the top electrode and bottom electrode respectively. All the electric measurements were measured using the electrochemical workstation CHI-660D at room temperature. An ordinary filament lamp with various power densities was used as light source. The spectrum of the light is shown in Fig. 2, which shows two peaks at

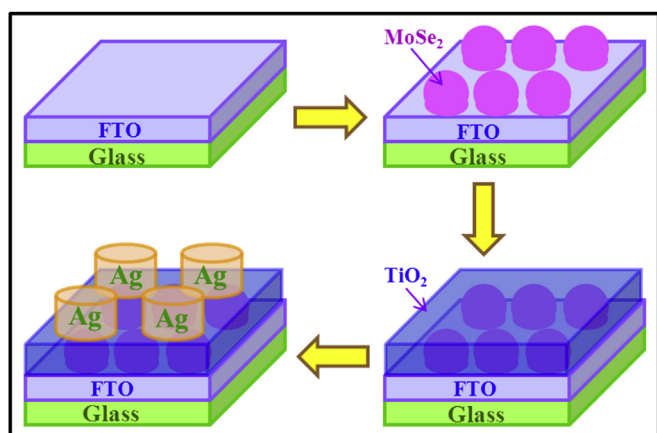


Fig. 1. Schematics fabrication of Ag/[MoSe₂/TiO₂]/FTO structure device with MoSe₂ nano-island array inserted into TiO₂ matrix grown on FTO substrate.

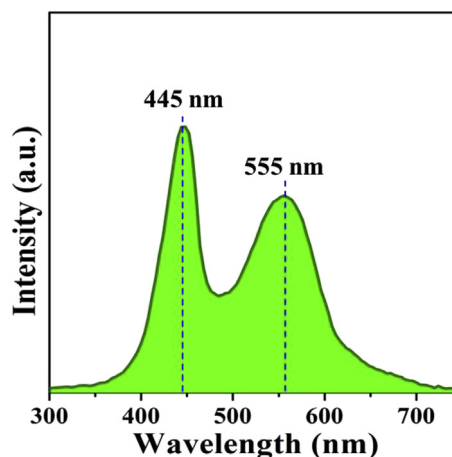


Fig. 2. The light spectra used as the light source in our experiment process.

~445 nm and ~555 nm, and the wavelength range of the light is 400–760 nm.

3. Results and discussion

Fig. 3(a) exhibits the scanning electron microscope (SEM) image of self-assembly MoSe₂ nano-islands array grown on FTO substrate. We can see that as-prepared sample consists of nano-islands array with the diameter of ~200 nm. The SEM image of anodic aluminum oxide (AAO) template is shown in the inset of Fig. 3(a). It is obvious that MoSe₂ nano-islands array inserted into TiO₂ matrix from transmission electron microscope (TEM) image in Fig. 3(b).

The crystalline compositions of as-prepared samples were characterized by XRD patterns. In order to make diffraction peaks of MoSe₂/TiO₂ composite clearer, we also present the XRD pattern of the pure FTO substrate without MoSe₂/TiO₂ composite. We can see that the crystallizations of TiO₂ and MoSe₂ are sufficiently without any other impurity phase from Fig. 3(c). Fig. 3(c) shows the X-ray powder diffraction (XRD) pattern of MoSe₂/TiO₂ compound at room temperature. The XRD profile of MoSe₂ powder matches very well with that in the reported work [30,31]. Obviously, all XRD peaks can be indexed to 2H–MoSe₂ structure. In addition, TiO₂ exhibits rutile phase (JCPDS: 211276). No other impurity peaks are detected. The low background and sharp peaks suggest that the MoSe₂ and TiO₂ retain their crystallinity. Moreover, the MoSe₂/TiO₂ composite were further confirmed by elemental analysis carried out from energy-dispersive X-ray (EDX) spectra, the EDX data in Fig. 3(d) confirms that the elements of composite are Mo, Se, Ti and O without any

other impurities.

Chemical compositions of MoSe₂/TiO₂ composite were investigated by X-ray photoelectron spectroscopy (XPS) analysis (Fig. 4). Mo 3d_{5/2} and Mo 3d_{3/2} were found at 229 and 232 eV confirming that molybdenum is in its Mo (IV) state; and the 3d peak of Se element is split into well-defined 3d_{5/2} and 3d_{3/2} peaks at 54.4 and 55.3 eV respectively. The residual carbon content in the matter was also a little higher although still in trace amount from Fig. 4(a). We can see that there were two peaks in the Ti 2p region, the peak located at 464.2 eV corresponded to Ti 2p_{1/2} and another one located at 458.6 eV was assigned to Ti 2p_{3/2}. The splitting between Ti 2p_{1/2} and Ti 2p_{3/2} was 5.7 eV, indicating a normal state of Ti⁴⁺ in the as-prepared MoSe₂/TiO₂ composite. The one peak of O 1s was related to Ti–O bonds (530.1 eV). The above XRD and XPS results confirmed the coexistence of MoSe₂ and TiO₂ in the MoSe₂/TiO₂ composite.

To check the capacitive performance of Ag/[MoSe₂/TiO₂]/FTO structure device, a typical current–voltage (I–V) response of heterostructure was investigated. Fig. 5(a) shows the experimental setup, in which Ag and FTO are the top and bottom electrode respectively, and an ordinary filament lamps with power density 60 mW/cm² is used as light source, where the wavelength range of white-light is 400–760 nm. The typical I–V characteristics curves of Ag/[MoSe₂/TiO₂]/FTO structure in dark and under light irradiation exhibit an asymmetric behavior with significant hysteresis (Fig. 5(b)). The arrows in the figure denote the sweeping directions of the applied voltage. An obvious bipolar resistive switching behavior with rapid conversion and good reproducibility in Ag/

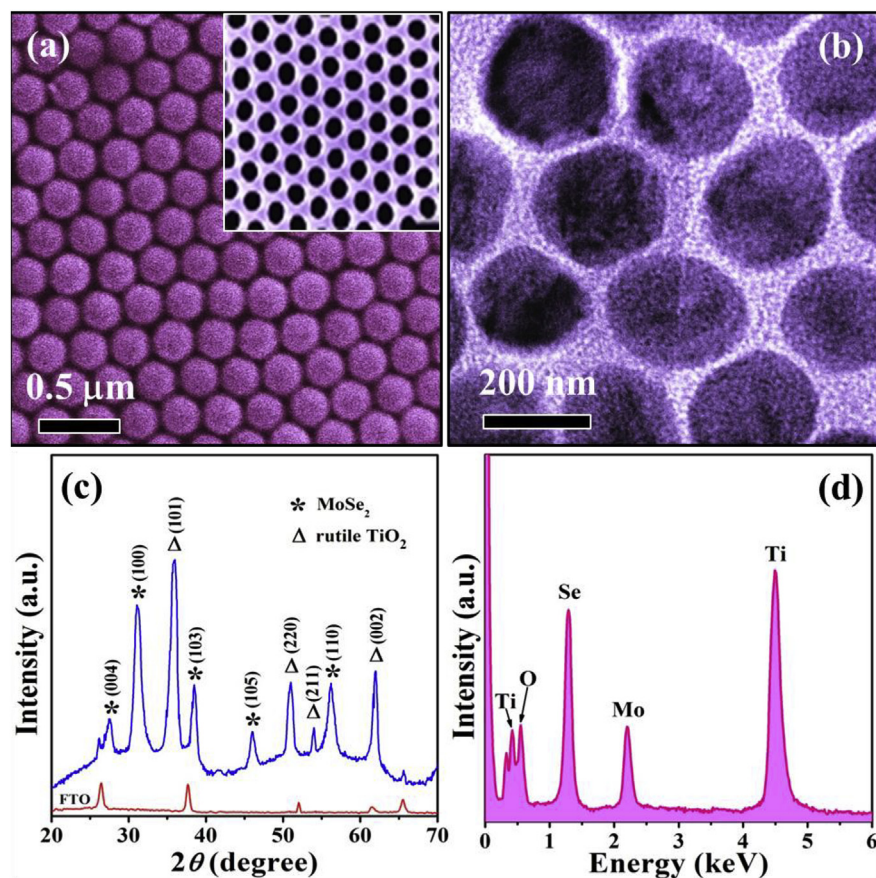


Fig. 3. (a) SEM image of MoSe₂ nano-islands array with a diameter of ~200 nm, the inset shows SEM image of anodic aluminum oxide (AAO) nano-template. (b) TEM image of MoSe₂/TiO₂ composite. (c) X-ray powder diffraction (XRD) patterns of MoSe₂/TiO₂ composite at room temperature. (d) Energy-dispersive X-ray (EDX) spectra of MoSe₂/TiO₂ composite.

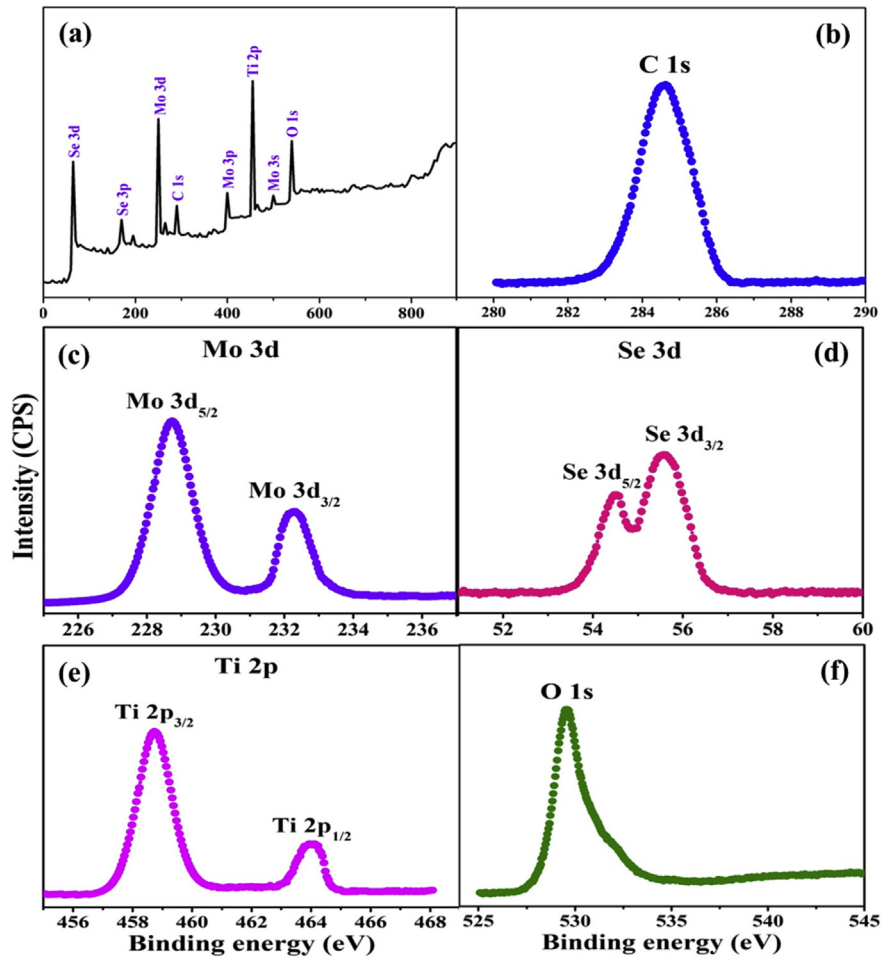


Fig. 4. (a) XPS survey spectra of MoSe₂/TiO₂ composite. (b) High resolution C 1s spectra. (c) High resolution Mo 3d spectra. (d) High resolution Se 3d spectra. (e) High resolution Ti 2p spectra. (f) High resolution O 1s spectra.

[MoSe₂/TiO₂]/FTO device is observed. To avoid electrical permanent breakdown for the devices, the compliance current (CC) of 25 μ A is used during the set and reset process.

Fig. 5(c) displays a prominent resistance switching effect in logarithmic scale. We can see that the device exhibits two stable resistance states when applying a positive electric field. It is obvious that a sudden current increase occurs at about 2.22 V (V_{Set}) in dark and 2.02 V (V_{Set}^1) under white-light illumination, indicating a “Set” process from a high resistance state (HRS) or “OFF” state to a low resistance state (LRS) or “ON” state happens. When the applied voltage sweeps from zero to a negative voltage of about -1.98 V (V_{Reset}) in dark and -1.79 V (V_{Reset}^1) under illumination, a “Reset” process from a low resistance state (LRS) or “ON” state to high resistance state (HRS) or “OFF” state occurs. The two well-resolved states provide a clear memory window of the device. More importantly, it is highly obvious that white-light illumination can regulate the resistive switching effect and magnify the memory windows, demonstrating the great potential of Ag/[MoSe₂/TiO₂]/FTO device for photo-controlled memory applications.

To evaluate the practical application of the resistive switching characteristics of Ag/[MoSe₂/TiO₂]/FTO device, the resistance-cycle number curves with a positive bias voltage of 1.0 V were tested and shown in Fig. 5(d). It is obvious that the resistance is about 1500 k Ω at HRS in dark and 640 k Ω at HRS under white-light illumination, suggesting the white-light illumination can change the resistance value for HRS. However, the resistance is about 142 k Ω at

LRS in dark and 65 k Ω at LRS under white-light illumination, which indicate the white-light illumination can reduce the resistance value for LRS. More importantly, the resistances of HRS and LRS in dark and under light irradiation are nearly unchanged after 50 successive cycles, illustrating that the resistive switching effects in dark and under light irradiation are highly stable. According to the above results, the steady photo-controlled bistable resistive switching behavior in Ag/[MoSe₂/TiO₂]/FTO device provides the potential for photo-controlled non-volatile memory applications.

It is well known that the non-volatile resistive switching random access memory (RRAM) is based the hysteresis I–V curves of a material. Fig. 6 display the memory application of I–V response curves of Ag/[MoSe₂/TiO₂]/FTO device, which is corresponding well to memristive switching behavior, indicating that the device could be reliably written, read, and erased during each step in dark (Fig. 6(a–d)) and under illumination with power density of 60 mW/cm² (Fig. 6(a’–d’)) respectively. In dark, the device display a well resistive switching behavior with an abrupt written voltage V_{write} of 2.22 V under the compliance current (CC) of 25 μ A. Then it displays a single LRS state with read behavior with operating voltage range from 1.45 V to -1.33 V. Next, the device can erase the storage information with an obvious erase voltage of -1.33 V, which is called V_{erase} . Finally, this device exhibit a correspondent HRS state with read behavior with operating voltage range from -1.95 V to 2.17 V again. If we call the LRS is logic “0”, then HRS is logic “1” for this device. Thus the device exhibit memristive switching. During the

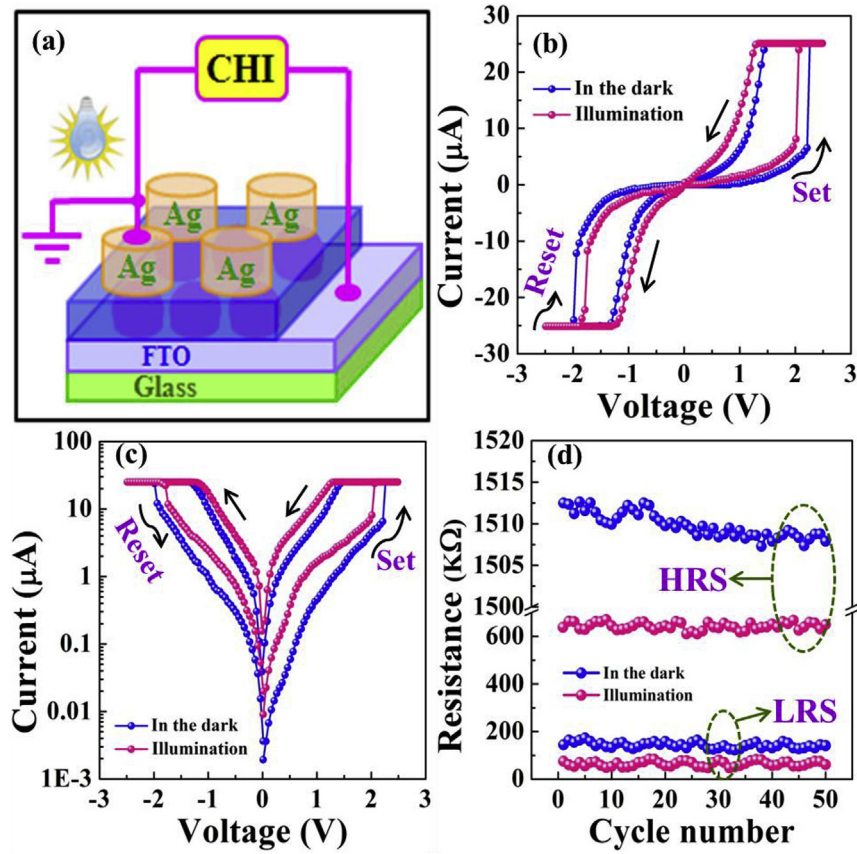


Fig. 5. (a) The experimental test circuit, Ag and FTO is top and bottom electrode respectively. (b) The typical current–voltage (I – V) characteristics of $\text{Ag}/[\text{MoSe}_2/\text{TiO}_2]/\text{FTO}$ structure. (c) The corresponding resistance switching effects in logarithmic scale. (d) The resistance–cycles curve with a positive bias voltage of 1.0 V.

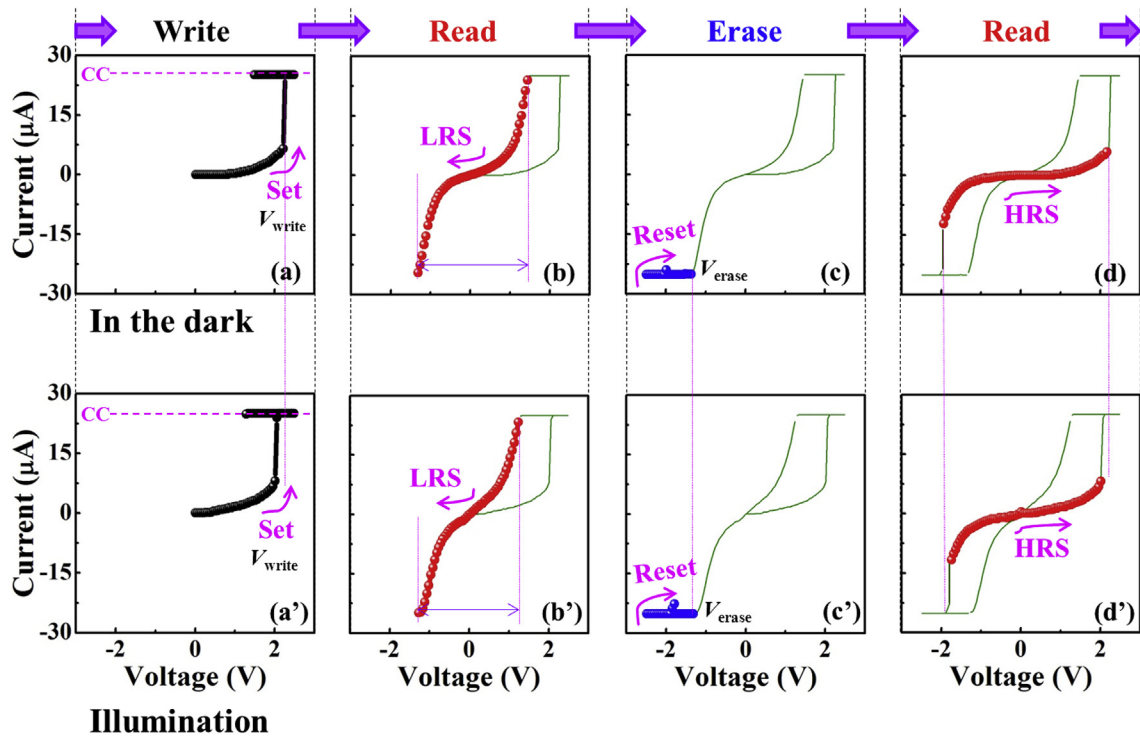


Fig. 6. The sequential write-read-erase-read operations yielded the corresponding I – V behaviors of the $\text{Ag}/[\text{MoSe}_2/\text{TiO}_2]/\text{FTO}$ device containing in dark and under white-light illumination respectively.

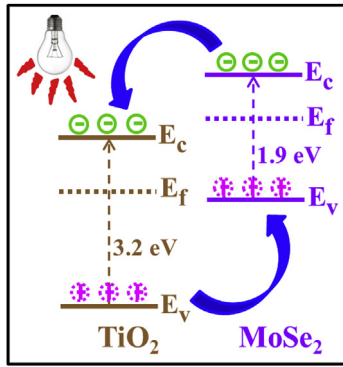


Fig. 7. A schematic of the electron–hole generation process of MoSe₂/TiO₂ composite under light illumination.

white-light illumination, it is greatly obvious that the V_{write} is become 1.98 V nearly, and the read behavior at LRS with operating voltage range from 1.22 V to -1.23 V. Moreover, the V_{erase} is also become -1.23 V. Further, the operating voltage of HRS state with read behavior range from -1.71 V to 1.98 V accordingly. Therefore, the resistive switching memory behaviors of Ag/[MoSe₂/TiO₂]/FTO device are useful in data storage technologies because they allow information to be written to the device once, and the data may not be subsequently erased or deleted from the device.

The mechanisms for resistive switching in metal/oxides/oxides structure have been extensively investigated [32]. It is generally believed that the electrically driven migration of the oxygen ions/vacancies plays a critical role in the operation of these devices [33–37]. In our works, the hysteresis loop I – V curve of Ag/[MoSe₂/TiO₂]/FTO device might be attributed to FTO as an oxygen guttering material to induce the oxygen vacancies at the [MoSe₂/TiO₂]/FTO interface with a Schottky-like barrier [38–51], which would modify the oxygen vacancies distribution within the device to result in the resistive switching characteristics [52–54]. Therefore, this bipolar resistive switching behavior should be result from the trapped and detrapped charge in the Schottky-like depletion layer [55]. The white-light illumination can modulate the resistive switching behavior by a large number of photogenerated charges, as shown in Fig. 7, which shows a schematic of the photogenerated charges transition between the valence band and the conduction band under light illumination. At room temperature, some of the electrons exist in the conductive band of MoSe₂ and TiO₂ due to thermal energy, which leads to good conductivity. When the light was turned on, the electrons in the valence band transit to the conduction band with the assistance of the phonons, and holes were generated in the valence band at the same time. Then the electrons will shift under the bias voltage, which leads to the photocurrent seen under light illumination. Due to the increasing of the photon densities, the probability of a transition between the valence band and the conduction band in the same part of the MoSe₂ and TiO₂ is increased. More electrons will shift under the bias voltage to form a current. Therefore, we observed a photo-controlled resistive switching memory effect in the [MoSe₂/TiO₂]/FTO device.

4. Conclusions

In conclusion, the MoSe₂/TiO₂ composite was prepared on FTO substrate, and a photo-controlled bipolar resistive switching memory characteristic based on Ag/[MoSe₂/TiO₂]/FTO device was observed. Our data indicates that the resistive switching effect in the Ag/[MoSe₂/TiO₂]/FTO structure results from the trapping-assisted carrier tunneling at the [MoSe₂/TiO₂]/FTO interface. The

superior resistive switching characteristics of Ag/[MoSe₂/TiO₂]/FTO hold great promise for next-generation photo-controlled nonvolatile memory applications.

Acknowledgments

This work was supported by Natural Science Foundation of Jiangsu Province (No. BK20150431), Research Foundation of Yancheng Institute of Technology (No. KJC2014004) and National Natural Science Foundation of China (No. 51202211).

References

- [1] D.S. Jeong, R. Thomas, R.S. Katiyar, J.F. Scott, H. Kohlstedt, A. Petraru, C.S. Hwang, Rep. Prog. Phys. 75 (2012) 076502.
- [2] C. Jin, J. Lee, E. Lee, E. Hwang, H. Lee, Chem. Commun. 48 (2012) 4235.
- [3] R. Waser, R. Dittmann, G. Staikov, K. Szot, Adv. Mater. 21 (2009) 2632.
- [4] H.J. Kim, Y.J. Baek, Y.J. Choi, C.J. Kang, H.H. Lee, H.M. Kim, K.B. Kim, T.S. Yoon, RSC Adv. 3 (2013) 20978.
- [5] H.G. Yoo, S. Kim, K.J. Lee, RSC Adv. 4 (2014) 20017.
- [6] J. Kolar, J.M. Macak, K. Terabe, T. Wagner, J. Mater. Chem. C 2 (2014) 349.
- [7] B. Sun, W. Zhao, L. Wei, H. Li, P. Chen, Chem. Commun. 50 (2014) 13142.
- [8] H. Borkar, A. Thakre, S.S. Kushvaha, R.P. Aloysius, A. Kumar, RSC Adv. 5 (2015) 35046.
- [9] B. Sun, Y. Liu, W. Zhao, J. Wu, P. Chen, Nano-Micro Lett. 7 (2015) 80.
- [10] B. Sun, C.M. Li, Phys. Chem. Chem. Phys. 17 (2015) 6718.
- [11] M. Ungureanu, R. Zazpe, F. Golmar, P. Stoliar, R. Llopis, F. Casanova, L.E. Hueso, Adv. Mater. 24 (2012) 2496.
- [12] M. Adachi, K. Yoshida, T. Kurata, J. Adachi, K. Tsuchiya, Y. Mori, F. Uchida, J. Mater. Res. 27 (2011) 440.
- [13] J. Park, S. Lee, J. Lee, K. Yong, Adv. Mater. 25 (2013) 6423.
- [14] J. Park, S. Lee, K. Yong, Nanotechnology 23 (2012) 385707.
- [15] Q.H. Wang, K.K. Zadeh, A. Kls, J.N. Coleman, M.S. Strano, Nat. Nanotechnol. 7 (2012) 699.
- [16] C. Fan, Z. Wei, S. Yang, J. Li, RSC Adv. 4 (2014) 775.
- [17] D. Duphil, S. Bastide, J.C. Rouchaud, J.L. Pastol, B. Legendre, C.L. Clemen, Nanotechnology 15 (2004) 828.
- [18] Y.D. Ma, Y. Dai, C.W. Niu, L. Yu, B.B. Huang, J. Phys. Chem. C 115 (2011) 202371.
- [19] S. Larents, B. Fallahzad, E. Tutuc, Appl. Phys. Lett. 101 (2012) 223104.
- [20] H.S. Lee, S.W. Min, Y.G. Chang, M.K. Park, T. Nam, H. Kim, J.H. Kim, S. Ryu, S. Im, Nano Lett. 12 (2012) 3695.
- [21] A. Ramasubramaniam, Phys. Rev. B Condens. Matter Phys. 86 (2012) 115409.
- [22] S.M. Delphine, M. Jayachandran, C. Sanjeeviraja, Crystallogr. Rev. 17 (2011) 281.
- [23] P.P. Hankare, A.A. Patil, K.M. Garadkar, D.J. Sathe, A.H. Manikshete, I.S. Mulla, J. Cryst. Growth 311 (2008) 15.
- [24] S.Y. Hu, Y.C. Lee, J.L. Shen, K.W. Chen, K.K. Tiong, Y.S. Huang, Solid State Commun. 139 (2006) 176.
- [25] D.A. Ras, G. Kostorz, D. Bremaud, M. Kalin, F.V. Kurdesau, A.N. Tiwari, M. Döbeli, Thin Solid Films 480 (2005) 433.
- [26] J.H. Zhan, Z.D. Zhang, X.F. Qian, C. Wang, Y. Xie, Y.T. Qian, Mater. Res. Bull. 34 (1999) 497.
- [27] K. Tang, Y. Qian, J.H. Zeng, X.G. Yang, Adv. Mater. 15 (2003) 448.
- [28] X.H. Chen, R. Fan, Chem. Mater. 13 (2001) 802.
- [29] G.G. Tang, J.R. Sun, C. Wei, K.Q. Wu, X.R. Ji, S.S. Liu, H. Tang, C.S. Li, Mater. Lett. 86 (2012) 9.
- [30] H. Shi, X. Zhou, Y. Lin, X. Fu, Mater. Lett. 62 (2008) 3649.
- [31] H. Tang, K. Dou, C.-C. Kaun, Q. Kuang, S. Yang, J. Mater. Chem. A 2 (2014) 360.
- [32] B. Sun, L. Wei, H. Li, X. Jia, J. Wu, P. Chen, J. Mater. Chem. C 3 (2015) 12149.
- [33] B. Sun, C.M. Li, Chem. Phys. Lett. 604 (2014) 127.
- [34] K. Nagashima, T. Yanagida, K. Oka, M. Kanai, A. Klamchuen, J.-S. Kim, B.H. Park, T. Kawai, Nano Lett. 11 (2011) 2114.
- [35] D.B. Strukov, G.S. Snider, D.R. Stewart, R.S. Williams, Nature 453 (2008) 80.
- [36] M.K. Yang, J.W. Park, T.K. Ko, J.K. Lee, Appl. Phys. Lett. 95 (2009) 042105.
- [37] P. Erhart, K. Albe, Appl. Phys. Lett. 88 (2006) 201918.
- [38] A. Sawa, T. Fujii, M. Kawasaki, Y. Tokura, Appl. Phys. Lett. 85 (2004) 1.
- [39] X.G. Chen, X.B. Ma, Y.B. Yang, L.P. Chen, G.C. Xiong, G.J. Lian, Y.C. Yang, J.B. Yang, Appl. Phys. Lett. 98 (2011) 122102.
- [40] J.K. Hyung, Y.J. Baek, Y.J. Choi, C.J. Kang, H.H. Lee, H.M. Kim, K.B. Kim, T.S. Yoon, RSC Adv. 3 (2013) 20978.
- [41] A. Shih, W. Zhou, J. Qiu, H.J. Yang, S. Chen, Z. Mi, I. Shih, Nanotechnology 21 (2010) 125201.
- [42] S. Hong, T. Choi, J.H. Jeon, Y. Kim, H. Lee, H.Y. Joo, I. Hwang, J.S. Kim, S.O. Kang, S.V. Kalinin, B.H. Park, Adv. Mater. 25 (2013) 2339.
- [43] B. Sun, J. Wu, X. Jia, F. Lou, P. Chen, J. Sol-Gel Sci. Technol. 16 (2015) 1573.
- [44] A. Sawa, T. Fujii, M. Kawasaki, Y. Tokura, Appl. Phys. Lett. 88 (2006) 232112.
- [45] B. Sun, Y. Liu, W. Zhao, P. Chen, RSC Adv. 5 (2015) 13513.
- [46] H. Sim, D.J. Seong, M. Chang, H. Hwang, J. Appl. Phys. 100 (2006) 88.
- [47] X.L. Deng, S. Hong, I. Hwang, J.S. Kim, J.H. Jeon, Y.C. Park, J. Lee, S.O. Kang,

- T. Kawai, B.H. Park, *Nanoscale* 4 (2012) 2029.
- [48] X.G. Chen, J.B. Fu, S.Q. Liu, Y.B. Yang, C.S. Wang, H.L. Du, G.C. Xiong, G.J. Lian, J.B. Yang, *Appl. Phys. Lett.* 101 (2012) 153509.
- [49] G. Chen, C. Song, C. Chen, S. Gao, F. Zeng, F. Pan, *Adv. Mater.* 24 (2012) 3515.
- [50] D. Rubi, F. Gomez-Marlasca, P. Bonville, D. Colson, P. Levy, *Phys. B* 407 (2012) 3144.
- [51] A. Sawa, T. Fujii, M. Kawasaki, Y. Tokura, *Appl. Phys. Lett.* 85 (2004) 18.
- [52] C.Y. Lin, C.Y. Wu, C.Y. Wu, T.C. Lee, F.L. Yang, C.M. Hu, T.Y. Tseng, *IEEE Electron Device Lett.* 28 (2007) 5.
- [53] R. Zazpe, M. Ungureanu, F. Golmar, P. Stolar, R. Llopis, F. Casanova, D.F. Pickup, C. Rogeroft, L.E. Hueso, *J. Mater. Chem. C* 2 (2014) 2013.
- [54] B. Sun, Y. Liu, F. Lou, P. Chen, *Chem. Phys.* 457 (2015) 28.
- [55] C.Y. Lin, D.Y. Lee, S.Y. Wang, C.C. Lin, T.Y. Tseng, *Surf. Coat. Technol.* 203 (2008) 628.